Coupling Dy_3 toroics in macrocycle

Qianqian Yang,[a, b] Jianfeng Wu,*[c] Chen Zhao,[a] Xu Ying,[a] Dong-Mei Zhu,[e] Xuefeng Guo,[c] Dan Liu,*[d] Yi-Quan Zhang,*[e] and Jinkui Tang*[a]

[a] State Key Laboratory of Rare Earth Resource Utilization, Changchun Institute of Applied Chemistry, Chinese Academy of Sciences, Changchun 130022, P. R. China. E-mail: tang@ciac.ac.cn.
[b] Xi'an Rare Metal Materials Institute Co., Ltd., Xi'an 710016, P. R. China.
[c] School of Chemistry and Chemical Engineering, Northwestern Polytechnical University, Xi'an, 710072, P. R. China. E-mail: jfwu@nwpu.edu.cn.
[d] School of Science, Changchun Institute of Technology, Changchun 130012, P. R. China. E-mail: danliusunshine@gmail.com.
[e] Ministry of Education Key Laboratory of NSLSCS, School of Physical Science and Technology, Nanjing Normal University, Nanjing 210023, P. R. China. E-mail: zhangyiquan@njnu.edu.cn.

1. Experimental section

General Synthetic Considerations.

All chemicals and solvents were commercially obtained without any further purification. Elemental analyses for C, H, and N were performed on a Elementar vario EL cube analyzer. FTIR spectra were obtained by a Nicolet 6700 Flex FTIR spectrometer in the range of 500-4000 cm^{-1} (Fig. S1). 3,3'-(propane-1,3-diylbis(oxy))bis(2-hydroxybenzaldehyde)[1] and 4,6-dihydrazinopyrimidine[2] were prepared by the previously published method.

Synthesis of 1. The complex has been synthesized by a "one-pot" strategy in which the macrocyclic ligand was generated in suit (Scheme S1). 4,6-dihydrazinopyrimidine (0.1 mmol) was dissolved in a mixed solvent of ethanol and acetonitrile (5 mL/10 mL). Then, $DyBr_3 \cdot 6H_2O$ (0.2 mmol) and 3,3'-(propane-1,3-diylbis(oxy))bis(2-hydroxybenzaldehyde) (0.1 mmol) were added to the mixture in sequence, and the reaction mixture was stirred for 10 min. Subsequently, triethylamine (0.15 mmol) was added to the mixture. After stirring for 6 h, the mixture was filtered to obtain yellow clarified filtrate. The filtrate was left un-disturb and allowed slow evaporation for one week. Yellow crystals of $[Dy_6(\mu_3\text{-}OH)_4(\mu_2\text{-}OH)_2LBr_2(H_2O)_{10}] \cdot Br_6 \cdot 2CH_3CH_2OH \cdot 2CH_3CN \cdot 2H_2O$ (**1**) were obtained for X-ray diffraction analysis. Yield: 21.1 mg, (21.5%, based on the metal salt). Elemental analysis (%) calcd for **1**: C, 20.40, H, 2.88, N, 6.66; found C, 20.13, H, 2.58, N, 6.39. IR (solid, ATR) $\tilde{\upsilon}$ [cm^{-1}] = 3166.54 (br), 1612.19 (s), 1560.13 (m), 1513.84 (m), 1498.41 (m), 1467.56 (s), 1450.21 (s), 1430.92 (m), 1400.06 (w), 1374.99 (w), 1321.03 (w), 1288.21 (m), 1216.86 (m), 1197.57 (s), 1170.57 (m), 1110.79 (w), 1091.51 (w), 1064.51 (m), 1052.94 (w), 1018.23 (w), 981.58 (w), 966.16 (w), 939.16 (w), 873.59 (w), 852.38 (w), 806.09 (w), 765.60 (m), 728.96 (m), 617.11 (w), 605.53 (w), 590.11 (w), 582.39 (w), 565.04 (m).

Crystallography

Single-crystal X-ray data of the complexes were collected on a Bruker D8 venture CCD diffractometer equipped with graphite-monochromatized Mo-Kα radiation (λ = 0.71073 Å). The structures were solved with SHELXT[3] and refined on *F*2 using all reflections with ShelXL[4] (full-matrix least-squares techniques) in the Olex2[5] package. All non-hydrogen atoms in the whole structure were refined with anisotropic displacement parameters. Hydrogen atoms were introduced in calculated positions and refined with fixed geometry with respect to their carrier atoms. The empirical formula and derived values are in accordance with the calculated cell content. In addition, for complex **1**, the checkcif report shows the unit cell still contains solvent-accessible voids, implying the existence of some solvent molecules in the structure that cannot be found from the weak residual electron peaks. These solvent molecules in the crystal data are highly disordered. A Solvent Mask routine of the Olex2 software was used to calculate and evaluate the possible disordered solvent molecules in the accessible voids of the crystal structure. The Solvent Mask result shows that *ca*. 236 electrons are located in a volume of 1048 $Å^3$ in one void per unit cell. Therefore, this is consistent with the presence of two ethanol, two acetonitrile, and two water molecules per asymmetric unit. Crystallographic data and selected bond parameters are shown in Tables S1 and S2. The crystal packing models of the complexes are shown in Fig. S2. CCDC 2411796 contains the supplementary crystallographic data for this paper. These data can be obtained free of charge from the Cambridge Crystallographic Data Centre via www.ccdc.cam.ac.uk/data_request/cif.

Magnetic Measurements

Magnetic susceptibility measurements were performed on a Quantum Design MPMS-XL7 SQUID magnetometer equipped with a 7 T magnet. The direct current (dc) magnetic susceptibility measurements were performed on polycrystalline samples in the temperature range of 2~300 K with an applied field of 1000 Oe. The field-dependent magnetizations for all complexes were measured in the field range of 0~7 T. The alternating current (ac) susceptibility measurements were investigated in a 3.0 Oe ac oscillating and zero dc fields. Diamagnetic corrections were made with Pascal's constants for all the constituent atoms as well as the contributions of the sample holder.

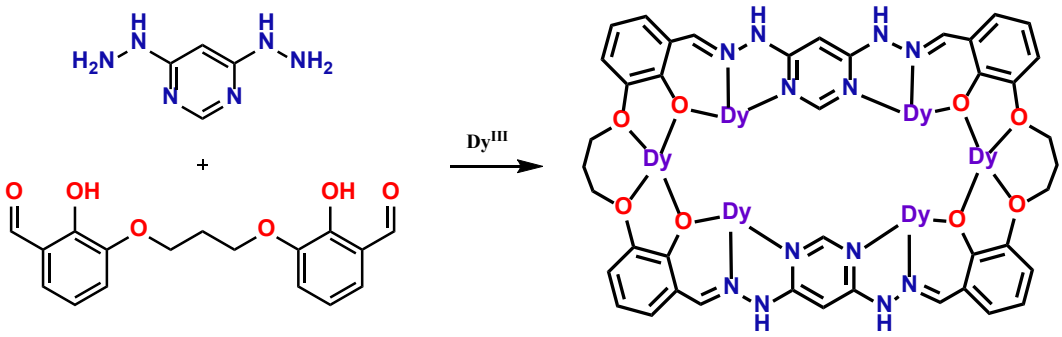

Scheme S1 Schematic drawing of the synthesis of complex **1** by a "one-pot" strategy.

2. IR spectroscopy

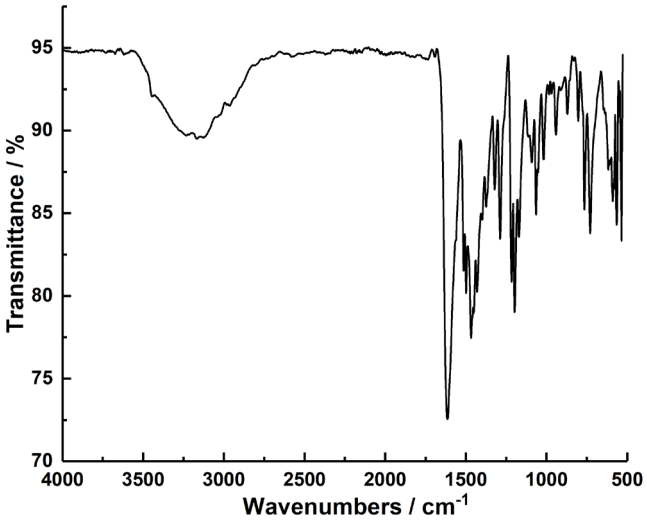

Fig. S1 IR (ATR) spectrum of solid samples for complex **1**.

3. Crystallographic details

Table S1 Crystallographic data for complex **1**.

	1
Formula	$C_{50}H_{84}Br_8Dy_6N_{14}O_{28}$
FW, g·mol^{-1}	2943.59
crystal system	monoclinic
space group	$P2_1/n$
T, K	150.0
λ, Å	0.71073
a, Å	11.9070(17)
b, Å	17.303(2)
c, Å	20.936(3)
α, °	90
β, °	97.553(4)
γ, °	90
V, Å^3	4276.1(10)
Z	2
ρ_{calcd}, g·cm^{-3}	2.286
GOF on F^2	1.036
reflns collected	41373
R_1 ($I \geq 2\ \sigma\ (I)$)	0.0683
wR_2 (all data)	0.1850
CCDC	2411796

Table S2 Selected bond distances (Å) and bond angles (°) for complex **1**.

Complex **1**					
Dy1-Br1	2.886(2)	Dy2-O3	2.314(9)	Dy3-O1[1]	2.431(10)
Dy1-O2	2.319(9)	Dy2-O5[1]	2.325(10)	Dy3-O2[1]	2.320(10)
Dy1-O5	2.342(9)	Dy2-O7	2.388(11)	Dy3-O3	2.345(11)
Dy1-O6	2.388(11)	Dy2-O8	2.390(10)	Dy3-O4	2.434(11)
Dy1-O7[1]	2.348(10)	Dy2-O9	2.399(12)	Dy3-O7	2.286(10)
Dy1-O8[1]	2.384(9)	Dy2-O10	2.360(13)	Dy3-O8	2.326(10)
Dy1-N1	2.530(13)	Dy2-N6	2.537(13)	Dy3-O11	2.359(13)
Dy1-N3	2.458(6)	Dy2-N4	2.471(6)	Dy3-O12	2.336(11)
O2-Dy1-Br1	95.8(3)	O3-Dy2-O7	73.1(4)	O1[1]-Dy3-O4	84.9(4)
O2-Dy1-O6	100.8(4)	O3-Dy2-O8	73.1(3)	O2[1]-Dy3-O8	73.5(3)
O2-Dy1-O7[1]	72.5(3)	O3-Dy2-O9	91.8(4)	O2[1]-Dy3-O11	99.8(4)
O2-Dy1-O8[1]	72.4(3)	O3-Dy2-O10	98.5(5)	O2[1]-Dy3-O12	90.8(4)
O2-Dy1-N1	73.0(4)	O3-Dy2-N6	72.4(4)	O3-Dy3-O11	91.8(5)
O5-Dy1-Br1	97.4(3)	O5[1]-Dy2-O7	76.4(3)	O7-Dy3-O1[1]	128.0(4)
O5-Dy1-O6	87.6(4)	O5[1]-Dy2-O8	74.5(3)	O7-Dy3-O2[1]	73.7(3)
O5-Dy1-O7[1]	76.9(3)	O5[1]-Dy2-O9	99.4(4)	O7-Dy3-O3	74.4(3)
O5-Dy1-O8[1]	74.3(3)	O5[1]-Dy2-O10	90.8(4)	O7-Dy3-O11	75.1(4)
O5-Dy1-N3	79.8(3)	O5[1]-Dy2-N4	80.2(3)	O8-Dy3-O1[1]	129.8(4)
O6-Dy1-N1	74.6(4)	O7-Dy2-O9	74.8(4)	O8-Dy3-O4	125.9(4)
O6-Dy1-N3	73.4(3)	O8-Dy2-N6	132.4(4)	O8-Dy3-O12	75.6(4)
O7-Dy1-Br1	76.2(3)	O9-Dy2-N6	77.2(4)	O11-Dy3-O1[1]	79.5(5)
O8-Dy1-O6	76.6(4)	O9-Dy2-N4	72.9(4)	O11-Dy3-O4	79.3(4)
O8-Dy1-N1	129.1(4)	O1-Dy2-O8	77.5(4)	O12-Dy3-O1[1]	75.3(4)
N1-Dy1-Br1	81.7(3)	O1-Dy2-N6	76.2(5)	O12-Dy3-O3	99.6(4)
N3-Dy1-Br1	73.8(2)	O1-Dy2-N4	78.1(4)	O12-Dy3-O4	76.4(4)

[1]1-X,1-Y,1-Z

Table S3 The corresponding distances (Å) and angles (°) of Dy_3 triangle in complex **1**.

	1
Dy1⋯Dy2	3.489
Dy1⋯Dy3	3.496
Dy2⋯Dy3	3.503
Dy1−Dy2−Dy3	60.012
Dy2−Dy3−Dy1	59.802
Dy3−Dy1−Dy2	60.192
Distance between the nearest Dy_3 edges	6.6083
Dihedral angle between two Dy_3 plans	0.7412

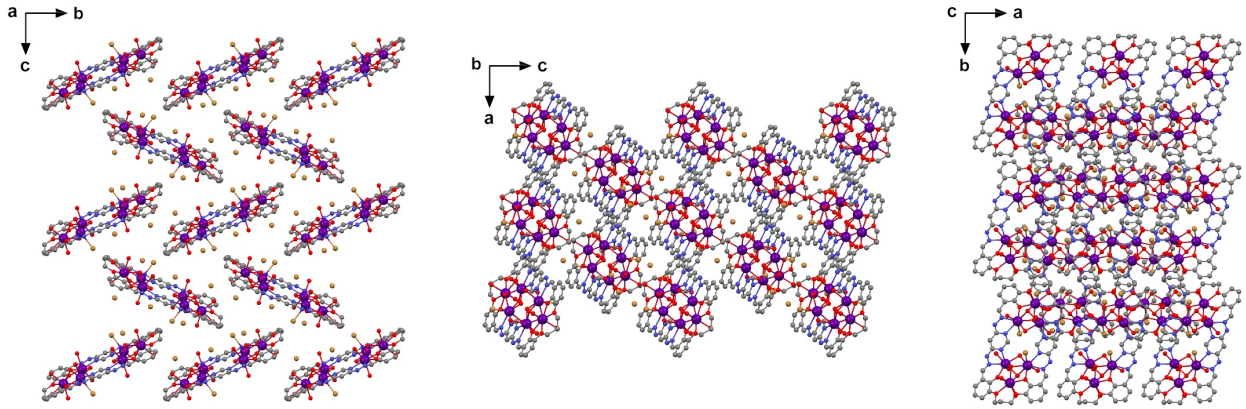

Fig. S2 Packing model along with a, b, and c axes of complex **1**. The purple, brown, blue, red and gray spheres represent Dy, Br, N, O, and C, respectively; hydrogen atoms have been omitted for clarity.

4. The *CShM* values calculations

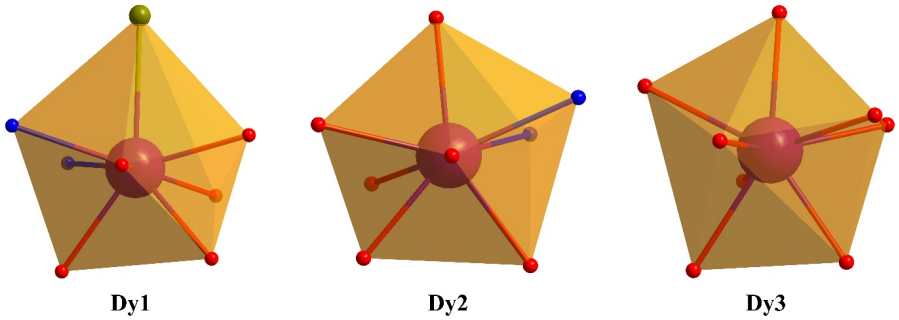

Fig. S3 Coordination polyhedrons of Dy^{III} ions in complex **1**. The purple, brown, blue and red spheres represent Dy, Br, N, and O, respectively.

Table S4 The *CShM* values calculated by *SHAPE* 2.1[6, 7] for complex **1**.

Coordination Geometry	Dy1	Dy2	Dy3
Hexagonal bipyramid (D_{6h})	16.251	15.636	15.835
Cube (O_h)	12.877	12.925	9.457
Square antiprism (D_{4d})	3.110	2.595	2.380
Triangular dodecahedron (D_{2d})	1.337	0.905	0.654
Johnson gyrobifastigium J26 (D_{2d})	13.356	11.830	14.820
Biaugmented trigonal prism J50 (C_{2v})	3.624	2.611	3.218
Biaugmented trigonal prism (C_{2v})	2.658	2.229	2.579
Snub diphenoid J84 (D_{2d})	3.573	2.112	3.218

5. Direct current (dc) magnetic susceptibility measurements

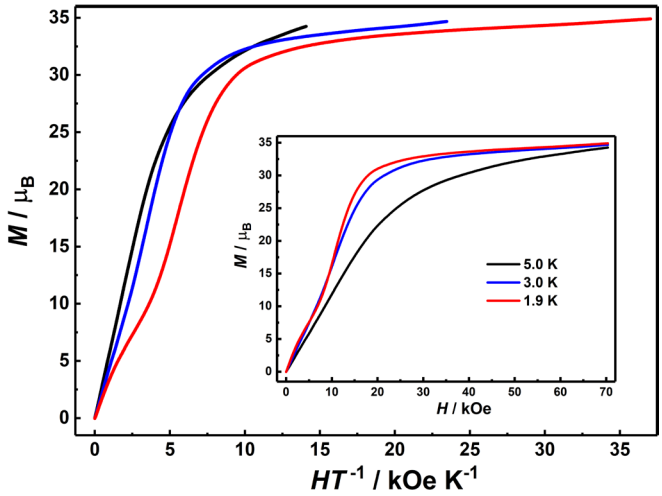

Fig. S4 Magnetization (*M*) versus *H*/*T* for complex **1** at indicated temperatures. Inset represents the plots of *M* versus *H*.

6. Alternating current (ac) magnetic susceptibility measurements

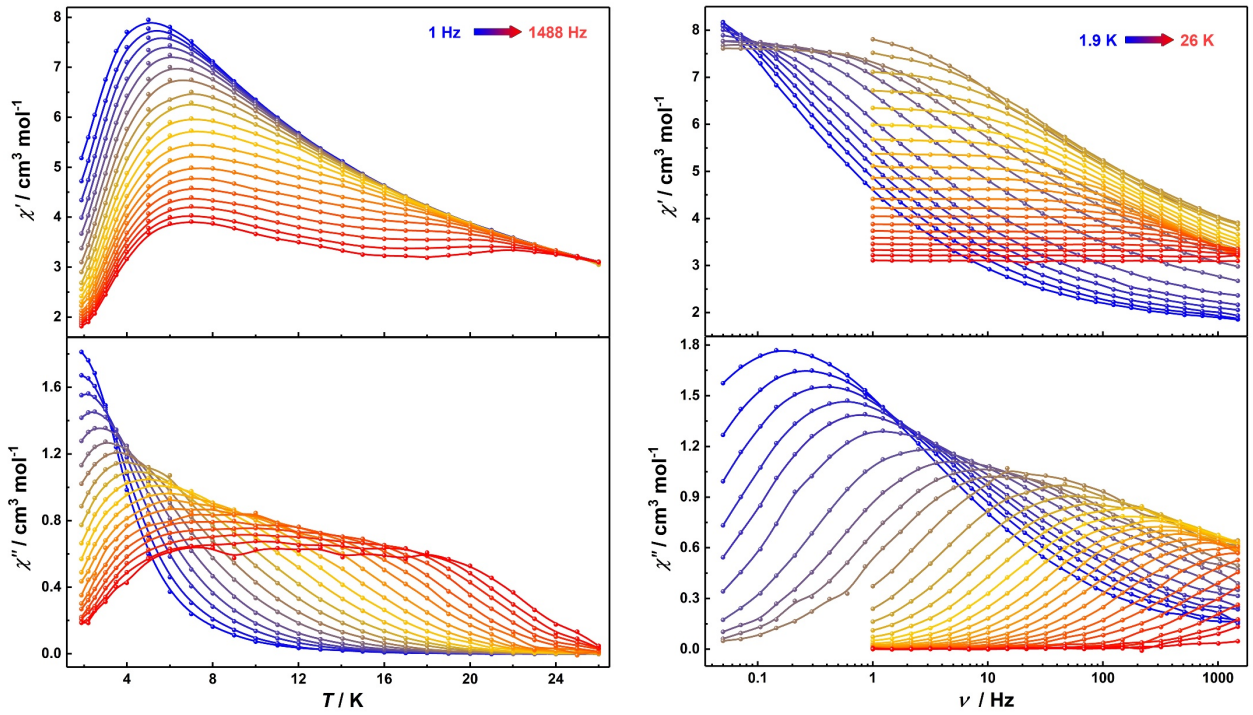

Fig. S5 Temperature-dependent (left) and frequency-dependent (right) ac susceptibility of complex **1** under zero dc field.

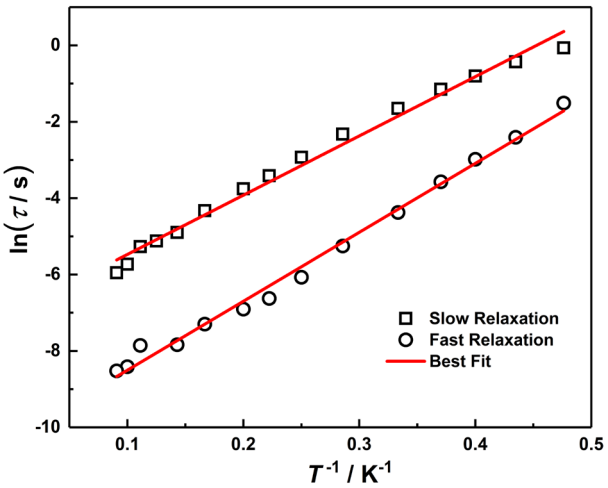

Fig. S6 Plot of lnτ vs. T^{-1} for complex **1** obtained under zero dc fields. The red line represents the best-fitted result.

Table S5 Parameters for the best fit of frequency-dependent ac susceptibility of complex **1** under zero dc field.

T/K	$\chi_{S,tot}$	$\Delta\chi_1$	α_1	$\Delta\chi_2$	α_2
2.1	1.72587	6.18486	0.56645	2.04315	0.27136
2.3	1.7612	5.01226	0.56183	2.54768	0.27625
2.5	1.82823	4.69075	0.55493	2.34295	0.23918
2.7	1.9124	4.26797	0.54647	2.36292	0.2381
3.0	2.04371	3.77135	0.54	2.43454	0.24692
3.5	2.32304	3.37899	0.51508	2.28231	0.23778
4.0	2.5188	3.00147	0.50154	2.37119	0.25879
4.5	2.65048	2.82737	0.48683	2.32372	0.26204
5.0	2.78344	2.76238	0.46626	2.14431	0.24643
6.0	2.87572	3.41111	0.54084	1.84569	0.24492
7.0	2.90316	2.62882	0.48734	2.15355	0.28436
8.0	2.97453	2.61157	0.45239	1.64359	0.23303
9.0	3.05635	2.47854	0.39761	1.25002	0.17419
10.0	2.84249	2.13093	0.37517	1.4176	0.19937
11.0	2.76028	2.021	0.34772	1.23951	0.17091

7. Computational details

Ab initio calculations were carried out with openMolcas[8], and are of CASSCF/RASSI-SO/SINGLE_ANISO type. For complex **1**, we only need to calculate three kinds of individual Dy^{III} fragments (**1**_Dy1, **1**_Dy2 and **1**_Dy3) due to the centrosymmetric molecular structure (see Fig. S7). Each of individual Dy^{III} fragments was calculated keeping the experimentally determined structure of the corresponding compound while replacing the other Dy^{III} ions with diamagnetic Lu^{III}. Two different basis-sets for all atoms are atomic natural orbitals from the ANO-RCC library (Table S6). The calculations employed the second order Douglas-Kroll-Hess Hamiltonian, where scalar relativistic contractions were taken into account in the basis set and the spin-orbit couplings were handled separately in the restricted active space state interaction (RASSI-SO) procedure.[9, 10] Active electrons in 7 active orbitals include all *f* electrons CAS(9 in 7) for Dy^{III} in the CASSCF calculations. To exclude all the doubts, we calculated all the roots in the active space. We have mixed the maximum number of spin-free state which was possible with our hardware (all from 21 sextets, 128 from 224 quadruplets, 130 from 490 doublets) for them. The SINGLE_ANISO[11-13] program was used to obtain the energy levels, *g* tensors, magnetic axes, *et al.* based on the above CASSCF/RASSI-SO calculations.

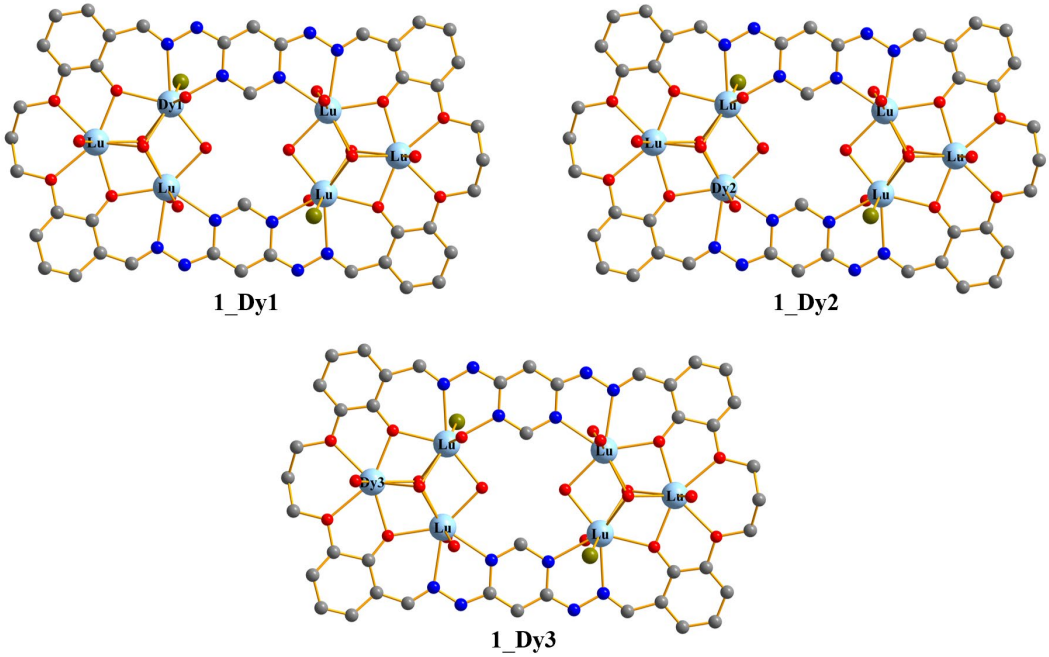

Fig. S7 Calculated model structures of individual Dy^{III} fragments of **1**; H atoms are omitted for clarify.

Table S6 Contractions of the employed basis sets in computational approximations.

	Basis set 1	Basis set 2
Dy	ANO-RCC-VDZP	ANO-RCC-VTZP
Lu	ANO-RCC-VDZ	ANO-RCC-VTZP
Br	ANO-RCC-VDZ	ANO-RCC-VTZ
N	ANO-RCC-VDZ	ANO-RCC-VTZ
O	ANO-RCC-VDZ	ANO-RCC-VTZ
C	ANO-RCC-VDZ	ANO-RCC-VDZ
H	ANO-RCC-VDZ	ANO-RCC-VDZ

Table S7 *Ab initio* energies (cm^{-1}) of the Kramers doublet for the ground Kramers doublet of each of the three dysprosium ions in complex **1** calculated based on the basis set 1.

	Dy1	Dy2	Dy3
KD1	0.0	0.0	0.0
KD2	28.2	26.0	149.9
KD3	137.9	96.4	187.6
KD4	187.4	161.8	233.7
KD5	245.1	224.1	258.3
KD6	305.2	296.3	284.8
KD7	417.6	408.5	295.9
KD8	528.0	473.7	492.5

Table S8 *Ab initio g* factors and orientation of the anisotropy axes for the ground Kramers doublet of each of the three dysprosium ions in complex **1** calculated based on the basis set 1.

	Dy1	Dy2	Dy3
g_X	0.32	0.50	0.03
g_Y	1.26	2.83	0.06
g_Z	18.58	16.59	19.56
Angle between anisotropy axis and the Dy_3 plane	2.749°	0.090°	2.316°

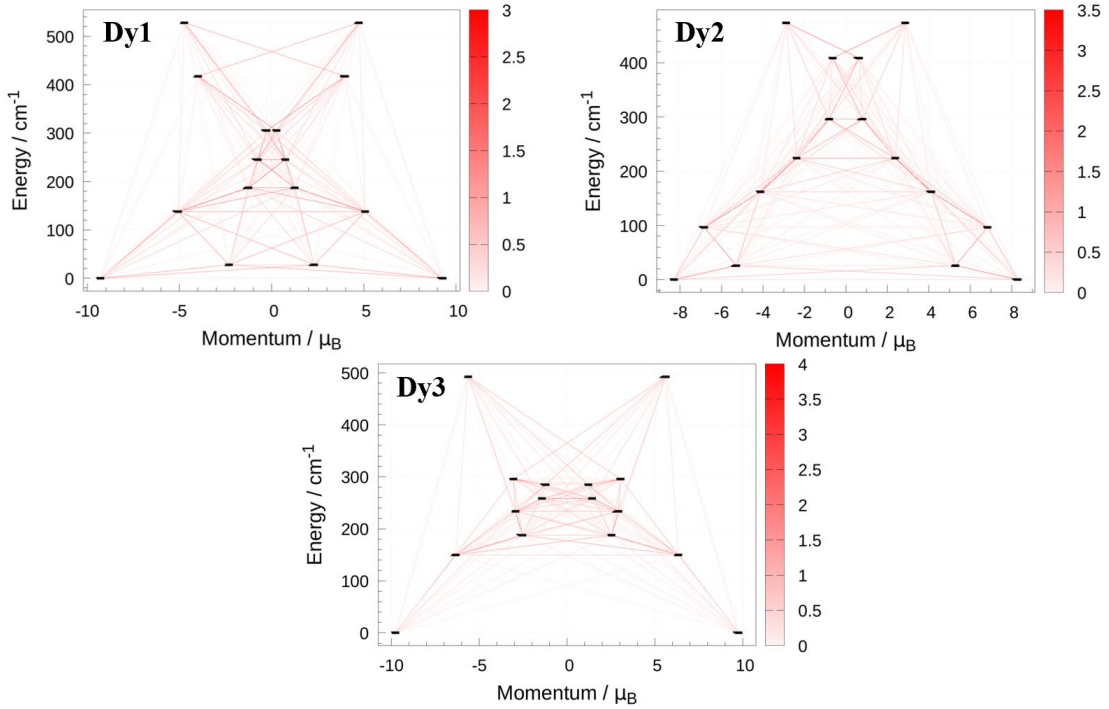

Fig. S8 The relaxations of magnetization blocking of Dy1, Dy2, and Dy3 in **1** calculated based on the basis set 1. The states are placed on the diagram according to their magnetic moments (bold black lines). The horizontal red lines show the tunneling transitions (the energy splitting) within each doublet state, while the nonhorizontal lines show the spin-phonon transition paths. The numbers at non-horizontal lines are averaged transition moments in μ_B connecting the corresponding states. The numbers at horizontal lines are tunneling gaps.

Table S9 Angles between anisotropy axes of the Dy^{III} ions in complex **1** calculated based on the basis set 1.

	Dy1	Dy2	Dy3
Dy1		128.679	94.812
Dy2	128.679		136.248
Dy3	94.812	136.248	

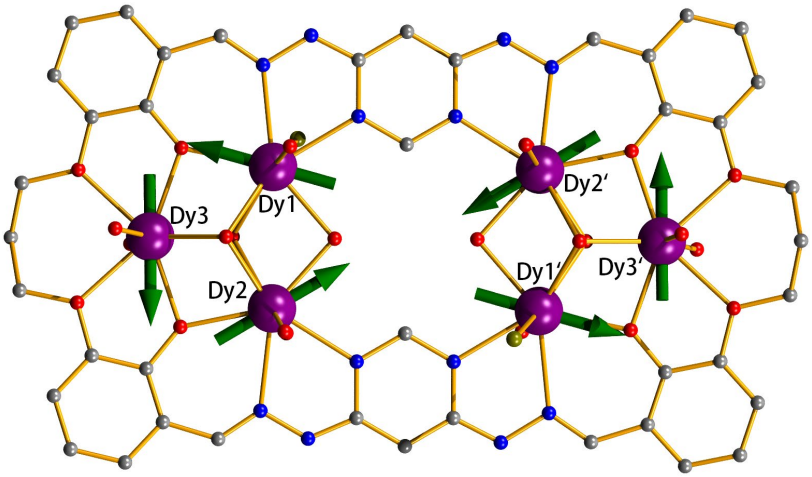

Fig. S9 Orientations of the main magnetic axes of the ground state of **1** calculated based on the basis set 1. All hydrogen atoms have been omitted for clarity.

Table S10 Calculated energy levels (cm^{-1}), g (g_x, g_y, g_z) tensors and predominant m_J values of the lowest eight Kramers doublets (KDs) of Dy1, Dy2 and Dy3 calculated based on the basis set 2.

KDs	Dy1			Dy2			Dy3		
	E	*g*	m_J	*E*	*g*	m_J	*E*	*g*	m_J
0	0.0	0.158 0.316 19.225	±15/2	0.0	0.054 0.132 19.461	±15/2	0.0	0.043 0.086 19.614	±15/2
1	66.4	1.048 1.429 17.178		63.5	0.218 0.344 19.435	±1/2	165.5	2.333 6.767 12.977	±13/2
2	108.8	0.034 2.020 15.004		155.9	1.914 2.314 14.302		207.2	3.227 5.094 7.427	
3	145.6	1.314 3.251 14.782		208.9	9.261 6.959 3.626		273.6	4.476 5.287 10.715	
4	176.3	2.517 4.623 11.283		251.2	2.004 2.535 12.603		317.7	0.020 0.616 17.147	
5	214.2	0.233 1.923 14.579		298.5	0.277 0.474 15.798		337.8	0.008 0.439 18.665	
6	268.3	0.199 0.328 18.603		404.4	0.055 0.111 18.861		376.5	0.158 0.275 19.089	
7	376.9	0.030 0.063 19.516		519.6	0.021 0.045 19.630		481.9	0.013 0.033 19.589	

Table S11 Wave functions with definite projection of the total moment | m_J > for the lowest eight KDs of Dy1, Dy2 and Dy3 calculated based on the basis set 2.

	E/cm^{-1}	wave functions
Dy1	0.0	91.5%|±15/2>
	66.4	39.3%|±1/2>+26.2%|±3/2>+14.2%|±5/2>+8.8%|±13/2>+4.4%|±7/2>
	108.8	58.3%|±13/2>+13.7%|±9/2>+7.9%|±11/2>+7.1%|±7/2>+7.0%|±1/2>
	145.6	24.2%|±5/2>+18.6%|±1/2>+16.8%|±7/2>+15.2%|±3/2>+10.1%|±9/2>+7.7%|±11/2>
	176.3	37.1%|±3/2>+21.6%|±1/2>+15.4%|±11/2>+12.5%|±5/2>+6.2%|±13/2>
	214.2	25.9%|±5/2>+24.9%|±7/2>+20.4%|±11/2>+12.2%|±9/2>+6.4%|±1/2>
	268.3	26.7%|±9/2>+23.1%|±7/2>+17.1%|±11/2>+7.5%|±3/2>+5.4%|±13/2>
	376.9	30.6%|±9/2>+23.8%|±11/2>+19.7%|±7/2>+9.2%|±13/2>+8.8%|±5/2>
Dy2	0.0	93.9%|±15/2>
	63.5	26.4%|±1/2>+24.9%|±3/2>+21.5%|±5/2>+13.4%|±7/2>+9.0%|±9/2>
	155.9	61.6%|±13/2>+17.7%|±9/2>+10.1%|±7/2>+5.5%|±3/2>
	208.9	26.9%|±1/2>+23.2%|±7/2>+19.6%|±11/2>+11.8%|±5/2>+7.6%|±13/2>+5.1%|±9/2>
	251.2	28.3%|±5/2>+25.3%|±3/2>+21.1%|±11/2>+8.6%|±13/2>+5.8%|±9/2>+4.9%|±1/2>
	298.5	31.4%|±1/2>+23.3%|±3/2>+16.9%|±11/2>+12.1%|±9/2>+7.8%|±13/2>
	404.4	24.2%|±7/2>+24.1%|±9/2>+17.0%|±5/2>+15.5%|±11/2>+8.3%|±3/2>+5.7%|±13/2>
	519.6	25.2%|±9/2>+22.1%|±7/2>+18.0%|±11/2>+14.2%|±5/2>+7.8%|±3/2>+6.8%|±13/2>
Dy3	0.0	96.3%|±15/2>
	165.5	34.7%|±13/2>+19.4%|±1/2>+14.8%|±5/2>+13.5%|±3/2>+9.5%|±9/2>
	207.1	46.3%|±13/2>+16.7%|±3/2>+14.5%|±1/2>+7.5%|±11/2>+7.2%|±9/2>
	273.6	31.9%|±11/2>+21.9%|±7/2>+14.1%|±5/2>+12.0%|±1/2>
	317.7	36.3%|±5/2>+25.2%|±3/2>+19.4%|±7/2>+6.6%|±11/2>+5.8%|±9/2>+5.8%|±1/2>
	337.8	30.5%|±9/2>+22.8%|±11/2>+16.7%|±7/2>+10.9%|±1/2>+6.6%|±13/2>+6.0%|±3/2>
	376.5	36.5%|±1/2>+28.6%|±3/2>+17.1%|±5/2>+9.3%|±7/2>
	481.9	29.0%|±9/2>+22.9%|±11/2>+21.5%|±7/2>+11.3%|±5/2>+8.7%|±13/2>

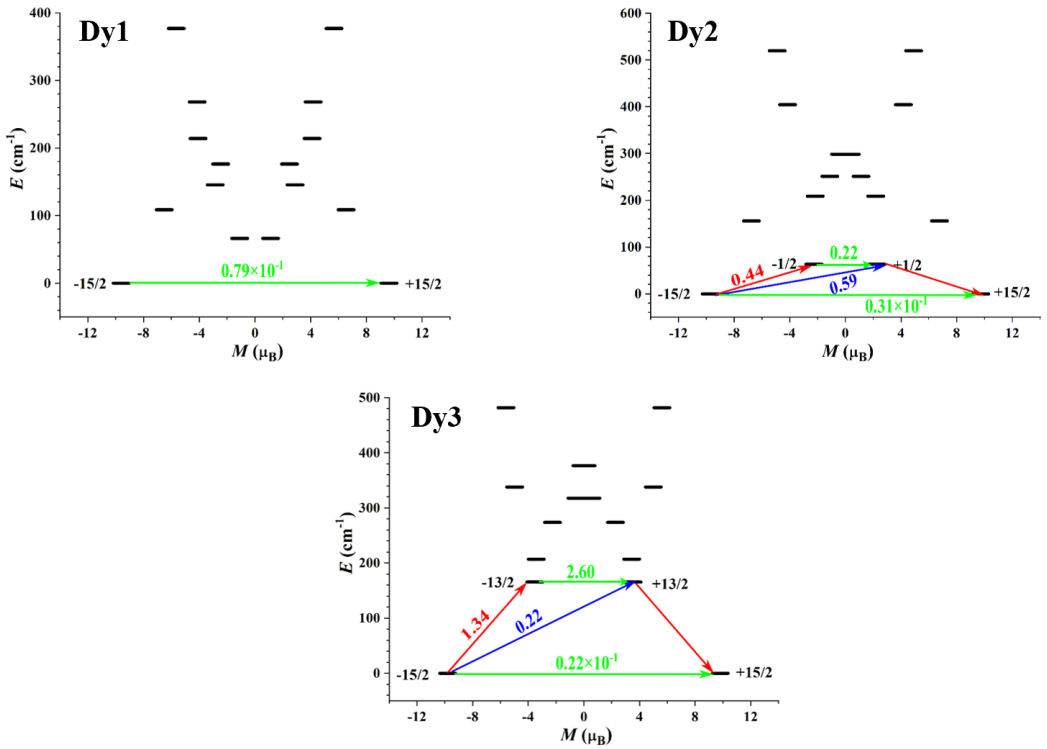

Fig. S10 Magnetization blocking barriers of complex **1** calculated based on the basis set 2. The thick black lines represent the KDs as a function of their magnetic moment along the magnetic axis. The blue lines correspond to diagonal matrix element of the transversal magnetic moment; the green lines represent Orbach relaxation processes. The path shown by the red arrows represents the most probable path for magnetic relaxation in the corresponding compounds. The numbers at each arrow stand for the mean absolute value of the corresponding matrix element of transition magnetic moment.

Table S12 Angles between anisotropy axes of the Dy^{III} ions in complex **1** calculated based on the basis set 2.

	Dy1	Dy2	Dy3
Dy1		107.4824	117.4337
Dy2	107.4824		134.9893
Dy3	117.4337	134.9893	

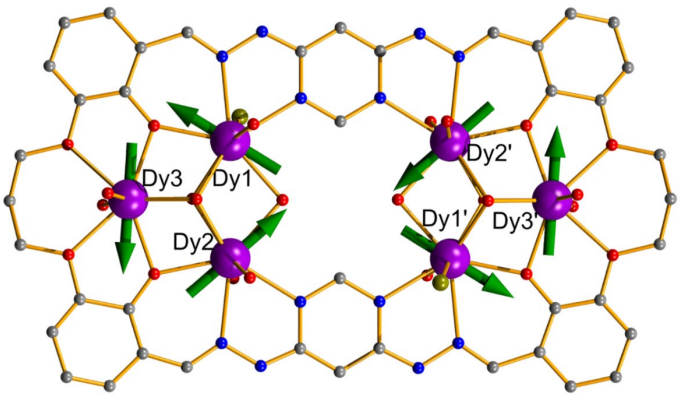

Fig. S11 Calculated orientations of the local main magnetic axes on Dy^{III} of complex **1** calculated based on the basis set 2.

To fit the exchange interactions between the magnetic centers in **1**, we took two steps to obtain them. Firstly, we calculated individual Dy^{III} fragments using CASSCF/RASSI-SO to obtain the corresponding magnetic properties. Then, the exchange interaction between the magnetic centers were considered within the Lines model,[14] while the account of the dipole-dipole magnetic coupling is treated exactly. The Lines model is effective and has been successfully used widely in the research field of *d* and *f*-elements single-molecule magnets.[15, 16]

For complex **1**, we only consider four types of $\tilde{J}$. The Ising exchange Hamiltonian is:

$$\hat{H}_{exch} = -\tilde{J}_1 [\hat{\tilde{S}}_{Dy_1}\hat{\tilde{S}}_{Dy_2} + \hat{\tilde{S}}_{Dy_1'}\hat{\tilde{S}}_{Dy_2'}] - \tilde{J}_2[\hat{\tilde{S}}_{Dy_1}\hat{\tilde{S}}_{Dy_3} + \hat{\tilde{S}}_{Dy_1'}\hat{\tilde{S}}_{Dy_3'}] - \tilde{J}_3[\hat{\tilde{S}}_{Dy_2}\hat{\tilde{S}}_{Dy_3} + \hat{\tilde{S}}_{Dy_2'}\hat{\tilde{S}}_{Dy_3'}] - \tilde{J}_4[\hat{\tilde{S}}_{Dy_1}\hat{\tilde{S}}_{Dy_2'} + \hat{\tilde{S}}_{Dy_1'}\hat{\tilde{S}}_{Dy_2}] \quad (1)$$

$\tilde{J} = 25J\cos\theta$, where θ is the angle between the magnetic axes on two Dy^{III} sites, and J is the Lines exchange coupling parameter. $\tilde{S}_{Dy} = 1/2$ is the ground pseudospin on the Dy^{III} site. $\tilde{J}_{total}$ is the parameter of the total magnetic interaction ($\tilde{J}_{total} = \tilde{J}_{dip} + \tilde{J}_{exch}$) between magnetic center ions. The dipolar magnetic coupling can be calculated exactly, while the exchange coupling constant was fitted through comparison of the computed and measured magnetic susceptibilities using the POLY_ANISO program.[11-13]

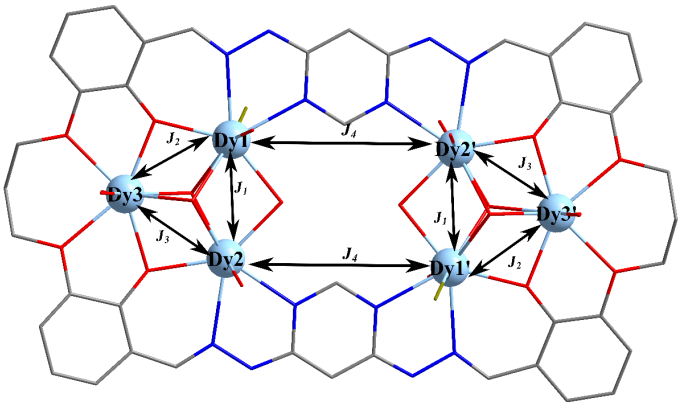

Fig. S12 Scheme of the Dy···Dy interactions in **1**.

Table S13 Dipolar coupling matrix from the direct calculation.

$$\tilde{J}_1 = \begin{pmatrix} 0.00 & 0.00 & 0.02 \\ 0.00 & 0.00 & 0.05 \\ 0.01 & 0.02 & 2.76 \end{pmatrix} \qquad \tilde{J}_2 = \begin{pmatrix} 0.00 & 0.00 & 0.01 \\ 0.00 & 0.00 & 0.02 \\ 0.00 & 0.01 & 1.32 \end{pmatrix}$$

$$\tilde{J}_3 = \begin{pmatrix} 0.00 & 0.00 & 0.00 \\ 0.00 & 0.00 & -0.01 \\ 0.00 & 0.00 & -1.08 \end{pmatrix} \qquad \tilde{J}_4 = \begin{pmatrix} 0.00 & 0.00 & 0.01 \\ 0.00 & 0.00 & 0.01 \\ 0.00 & 0.00 & 0.90 \end{pmatrix}$$

Table S14 The exact $\tilde{J}$ tensors in the dipolar coupling matrix from the direct calculation.

	$\tilde{J}_1$	$\tilde{J}_2$	$\tilde{J}_3$	$\tilde{J}_4$
$\tilde{J}_{xx}$	6.31×10^{-5}	2.37×10^{-5}	-6.60×10^{-6}	2.05×10^{-5}
$\tilde{J}_{xy}$	1.54×10^{-4}	4.74×10^{-5}	-1.30×10^{-5}	5.01×10^{-5}
$\tilde{J}_{xz}$	2.27×10^{-2}	1.08×10^{-2}	-2.99×10^{-3}	7.38×10^{-3}
$\tilde{J}_{yx}$	1.26×10^{-4}	5.95×10^{-5}	-1.60×10^{-5}	4.10×10^{-5}
$\tilde{J}_{yy}$	3.09×10^{-4}	9.48×10^{-5}	-3.20×10^{-5}	1.00×10^{-4}
$\tilde{J}_{yz}$	4.55×10^{-2}	2.16×10^{-2}	-7.31×10^{-3}	1.48×10^{-2}
$\tilde{J}_{zx}$	7.68×10^{-3}	2.88×10^{-3}	-2.36×10^{-3}	1.98×10^{-3}
$\tilde{J}_{zy}$	1.87×10^{-2}	5.77×10^{-3}	-4.72×10^{-3}	3.97×10^{-3}
$\tilde{J}_{zz}$	2.76	1.32	−1.08	0.90

Table S15 Fitted exchange couplings $\tilde{J}_{exch}$, the calculated dipole-dipole interaction $\tilde{J}_{dip}$ and the total constants $\tilde{J}_{total}$ between magnetic center ions in **1**. The intermolecular interactions zJ' of **1** was fitted to −0.05 cm^{-1}.

	$\tilde{J}_{exch}$	$\tilde{J}_{dip}$	$\tilde{J}_{total}$
$\tilde{J}_1$	−1.88	2.76	0.88
$\tilde{J}_2$	−2.88	1.32	−1.56
$\tilde{J}_3$	−4.42	−1.08	−5.50
$\tilde{J}_4$	0.38	0.90	1.28

Table S16 Exchange energies E (cm^{-1}), the energy difference between each exchange doublets Δ_t (cm^{-1}) and the main values of the g_z for the lowest 32 exchange doublets of complex **1**.

	E	Δ_t	g_z		E	Δ_t	g_z
0	0.00000000000 0.00000000147	0.147×10^{-8}	29.233	16	4.84550876048 4.84550876252	0.204×10^{-8}	38.081
1	0.21754706192 0.21754706533	0.341×10^{-8}	38.272	17	5.01856738670 5.01856738797	0.127×10^{-8}	66.118
2	0.54539116825 0.54539117140	0.314×10^{-8}	9.038	18	5.21669866599 5.21669866926	0.327×10^{-8}	61.118
3	0.73425958061 0.73425958274	0.213×10^{-8}	27.181	19	5.22578003508 5.22578003875	0.367×10^{-8}	39.381
4	0.79050921960 0.79050922672	0.712×10^{-8}	1.373	20	5.28676073469 5.28676074202	0.733×10^{-8}	78.350
5	0.80413855609 0.80413856187	0.578×10^{-8}	9.781	21	5.38188333703 5.38188334180	0.477×10^{-8}	39.796
6	1.52946172228 1.52946172399	0.171×10^{-8}	38.363	22	5.60234653342 5.60234653648	0.306×10^{-8}	38.897
7	1.57402006490 1.57402006972	0.482×10^{-8}	40.137	23	5.66739944603 5.66739944910	0.307×10^{-8}	39.224
8	3.42773476118 3.42773476348	0.229×10^{-8}	38.885	24	7.43034501008 7.43034501054	0.460×10^{-9}	0.080
9	3.64571610205 3.64571610358	0.153×10^{-8}	38.873	25	8.09586604865 8.09586605187	0.322×10^{-8}	39.127
10	4.06784413664 4.06784413796	0.132×10^{-8}	29.838	26	8.54960918532 8.54960919016	0.484×10^{-8}	72.182
11	4.23116769318 4.23116769722	0.404×10^{-8}	61.956	27	8.66848330939 8.66848331248	0.309×10^{-8}	83.230
12	4.24018803949 4.24018804124	0.175×10^{-8}	67.974	28	8.97662113546 8.97662113800	0.254×10^{-8}	38.329
13	4.36987619845 4.36987619888	0.430×10^{-9}	45.633	29	9.01461616048 9.01461616232	0.184×10^{-8}	66.275
14	4.66359302172 4.66359302680	0.508×10^{-8}	71.879	30	9.57179111856 9.57179111996	0.140×10^{-8}	38.257
15	4.74282622226 4.74282622296	0.700×10^{-9}	43.419	31	10.40245386601 10.40245386628	0.270×10^{-9}	0.056

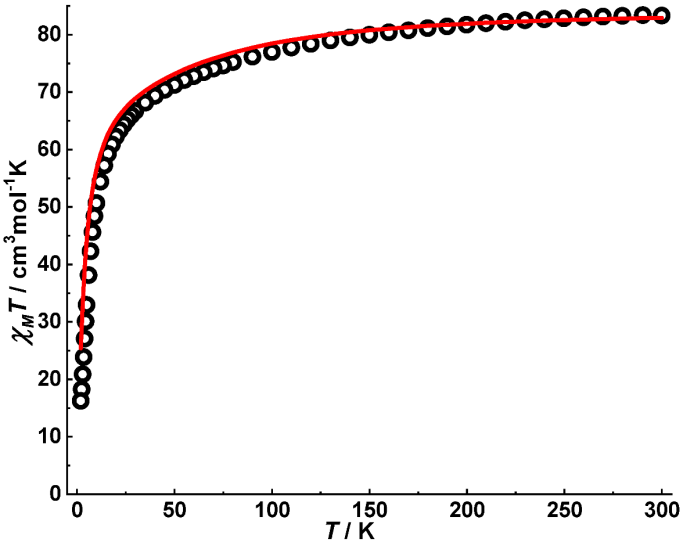

Fig. S13 Calculated (red solid line) and experimental (black square dot) data of magnetic susceptibility of complex **1**. The intermolecular interaction zJ' of complex **1** was fitted to –0.05 cm^{-1}.

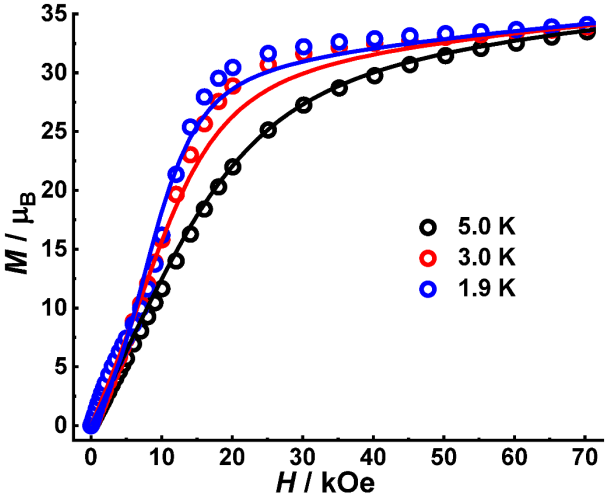

Fig. S14 Experimental (dots) and calculated (lines) magnetic susceptibilities for **1**.

8. References

1. L. Carbonaro, M. Isola, V. Liuzzo, F. Marchetti, F. Balzano, C. Silvio Pomelli and A. Raffaelli, *Eur. J. Inorg. Chem.*, 2001, **2001**, 353-357.
2. M. B. Bushuev, V. P. Krivopalov, N. V. Semikolenova, Y. G. Shvedenkov, L. A. Sheludyakova, G. G. Moskalenko, L. G. Lavrenova, V. A. Zakharov and S. V. Larionov, *Russ. J. Coord. Chem.*, 2007, **33**, 601-606.
3. G. Sheldrick, *Acta Crystallogr. Sect. A*, 2015, **71**, 3-8.
4. G. Sheldrick, *Acta Crystallogr. Sect. C*, 2015, **71**, 3-8.
5. O. V. Dolomanov, L. J. Bourhis, R. J. Gildea, J. A. K. Howard and H. Puschmann, *J. Appl. Crystallogr.*, 2009, **42**, 339-341.
6. D. Casanova, M. Llunell, P. Alemany and S. Alvarez, *Chem. Eur. J.*, 2005, **11**, 1479-1494.
7. D. Casanova, P. Alemany, J. M. Bofill and S. Alvarez, *Chem. Eur. J.*, 2003, **9**, 1281-1295.
8. I. Fdez. Galván, M. Vacher, A. Alavi, C. Angeli, F. Aquilante, J. Autschbach, J. J. Bao, S. I. Bokarev, N. A. Bogdanov, R. K. Carlson, L. F. Chibotaru, J. Creutzberg, N. Dattani, M. G. Delcey, S. S. Dong, A. Dreuw, L. Freitag, L. M. Frutos, L. Gagliardi, F. Gendron, A. Giussani, L. González, G. Grell, M. Guo, C. E. Hoyer, M. Johansson, S. Keller, S. Knecht, G. Kovačević, E. Källman, G. Li Manni, M. Lundberg, Y. Ma, S. Mai, J. P. Malhado, P. Å. Malmqvist, P. Marquetand, S. A. Mewes, J. Norell, M. Olivucci, M. Oppel, Q. M. Phung, K. Pierloot, F. Plasser, M. Reiher, A. M. Sand, I. Schapiro, P. Sharma, C. J. Stein, L. K. Sørensen, D. G. Truhlar, M. Ugandi, L. Ungur, A. Valentini, S. Vancoillie, V. Veryazov, O. Weser, T. A. Wesołowski, P.-O. Widmark, S. Wouters, A. Zech, J. P. Zobel and R. Lindh, *J. Chem. Theory Comput.*, 2019, **15**, 5925-5964.
9. P. Å. Malmqvist, B. O. Roos and B. Schimmelpfennig, *Chem. Phys. Lett.*, 2002, **357**, 230-240.
10. B. A. Heß, C. M. Marian, U. Wahlgren and O. Gropen, *Chem. Phys. Lett.*, 1996, **251**, 365-371.
11. L. F. Chibotaru, L. Ungur, C. Aronica, H. Elmoll, G. Pilet and D. Luneau, *Journal of the American Chemical Society*, 2008, **130**, 12445-12455.
12. L. F. Chibotaru, L. Ungur and A. Soncini, *Angew. Chem. Int. Ed.*, 2008, **47**, 4126-4129.
13. L. Ungur, W. Van den Heuvel and L. F. Chibotaru, *New J. Chem.*, 2009, **33**, 1224-1230.
14. M. E. Lines, *J. Chem. Phys.*, 1971, **55**, 2977-2984.
15. K. C. Mondal, A. Sundt, Y. Lan, G. E. Kostakis, O. Waldmann, L. Ungur, L. F. Chibotaru, C. E. Anson and A. K. Powell, 2012, **51**, 7550-7554.
16. S. K. Langley, D. P. Wielechowski, V. Vieru, N. F. Chilton, B. Moubaraki, B. F. Abrahams, L. F. Chibotaru and K. S. Murray, *Angew. Chem. Int. Ed.*, 2013, **52**, 12014-12019.